Journal of Power Sources 206 (2012) 349–356

Contents lists available at SciVerse ScienceDirect

Journal of Power Sources

journal homepage: www.elsevier.com/locate/jpowsour

# Three-dimensional thermal modeling of a lithium-ion battery pack

Hongguang Sun*, Xiaohui Wang, Brian Tossan, Regan Dixon

*Canadian Regional Engineering Centre, GM of Canada Ltd. – General Motors Company, 1908 Colonel Sam Drive, Oshawa, ON, L1H 8P7, Canada*

ARTICLE INFO

*Article history:*
Received 31 October 2011
Received in revised form 10 January 2012
Accepted 12 January 2012
Available online 21 January 2012

*Keywords:*
Battery pack
Thermal model
Heat generation rate
Temperature uniformity

ABSTRACT

A three-dimensional thermal model has been developed to gain better understanding of thermal behavior of battery cells in a pack under simulated driving cycles. The numerical approach incorporates a three-dimensional CFD pack-level sub-model, a one-dimensional battery pack network sub-model, and a three-dimensional thermal and electrochemical coupled cell/module level sub-model so that the battery non-uniform heat generation rate, the battery temperature distribution as well as battery temperature variation across a pack can be quickly predicted. In particular, the flow profiles of each individual battery cooling channel are calculated using the three-dimensional CFD sub-model. Using the predicted flow profiles of the cooling channel as flow boundary conditions the thermal behavior of battery cells is predicted using the one-dimensional battery pack network sub-model and the cell/module level thermal sub-model, in which both electrochemical reaction and double layer effect of battery cells are considered. The thermal behavior of battery cells is correlated through physical tests. Finally, the effects of the cooling flow of battery pack and the design of battery pack cooling system on non-uniformity of individual battery cell temperature and battery cell temperature variation across the pack under simulated US06 driving cycles are studied and discussed.



## 1. Introduction

Rechargeable lithium-ion battery pack continues to be considered as a clean, efficient, and environmentally responsible power source for electric vehicles and various other applications. Major thermal concerns of a battery pack are overheating and uneven heating within each individual battery cell and across the entire battery pack during charge/discharge cycles, which can lead to fast battery degradation and capacity reduction of battery cells. Battery pack designs in which battery cells operate in controlled temperature ranges are desirable. Mathematical modeling of battery thermal behavior as well as cooling strategy has proven to be an efficient and cost effective tool to improve battery pack performance and extend durability.

Various mathematical models have been developed principally based on porous-electrode theory [1] to describe the charge/discharge of rechargeable battery cells. Notably, Wang et al. developed a micro-macroscopic coupled model to predict battery charge and discharge behaviors. In their works, microscopic conservation equations of species and charge and Bulter–Volmer equation were applied to describe the relationship among the concentration of species, potentials in solid and liquid phases, and the charge transfer. The battery cell current density and potential were predicted using a macroscopic cell model developed based on microscopic equations using local volume average technique [2]. The battery heat generation rate could be calculated based on current density, potential, and corresponding open-circuit potential [3]. However, due to the computational model size it requires significant time to complete battery cell level simulation based on real vehicle drive schedules using current-state computing hardware, though a reduced-order battery model based on proper orthogonal decomposition for lithium-ion battery simulations was introduced by Cai and White [4] to reduce the computing time.

Recently, an efficient and simplified two-dimensional battery thermal model was developed by Shin et al. [5,6] to significantly reduce the computing time. Based on the continuity of current density, $J$, on electrodes and Ohm's law the governing equations of positive electrode potential, $V_p$, and negative electrode potential, $V_n$, were derived as follows:

$$\nabla^2 V_p = -r_p J \tag{1}$$

$$\nabla^2 V_n = r_n J \tag{2}$$

where $r_p$ and $r_n$ were the resistances of positive electrode and negative electrode, respectively. They adopted the polarization expression proposed by Newman and Tiedemann [7] to describe the relation between current density and electrode potentials

$$J = Y(V_p - V_n - U) \tag{3}$$

* Corresponding author. Tel.: +1 905 6442624; fax: +1 905 6444932.
*E-mail address:* hongguang.sun@gm.com (H. Sun).

0378-7753/$ – see front matter © 2012 Elsevier B.V. All rights reserved.
doi:10.1016/j.jpowsour.2012.01.081

**Nomenclature**

| | |
|---|---|
| $a$ | specific area of battery cell, $m^{-1}$ |
| $a_p$ | specific area of positive electrode, $m^{-1}$ |
| $a_n$ | specific area of negative electrode, $m^{-1}$ |
| $A_e$ | area of cell active material surface, $m^2$ |
| $A_{pt}$ | area of battery cooling plate surface, $m^2$ |
| $A_t$ | cross section area of battery cell terminal tab, $m^2$ |
| $C$ | capacitance at battery equivalent circuit model, $F$ |
| $C_0 \sim C_6$ | dimensionless constants |
| $C_{p,c}$ | specific heat of battery cell, $J\,kg^{-1}\,K^{-1}$ |
| $C_{p,pt}$ | specific heat of battery holder, $J\,kg^{-1}\,K^{-1}$ |
| $C_p$ | coefficient of heat generation rate, DOD depth of discharge (dimensionless) |
| $h_a$ | lumped heat transfer coefficient of cooling plate, $W\,m^{-2}\,K^{-1}$ |
| $I$ | current, A |
| $I_c$ | capacitor current, A |
| $J$ | current density, $A\,m^{-2}$ |
| $K_{pt}$ | equivalent heat conductivity of battery cooling plate, $W\,m^{-1}\,K^{-1}$ |
| $K_t$ | heat conductivity of battery cell terminal tab, $W\,m^{-1}\,K^{-1}$ |
| $L_e$ | distance between centerlines of positive and negative electrode current collectors, m |
| $L_{pt}$ | thickness of battery holder, m |
| $L_t$ | length of battery cell terminal tab, m |
| $m_c$ | mass of a battery cell, kg |
| $m_{pt}$ | mass of battery cooling plate of a cell, kg |
| $N$ | number of separators in a cell (dimensionless) |
| $P$ | power input/output of a battery cell, W |
| $q''$ | heat generation rate of battery active material, $W\,m^{-3}$ |
| $R$ | battery resistance, Ω |
| $R_1$ | resistance of resistor 1 at battery equivalent circuit model, Ω |
| $R_2$ | resistance of resistor 2 at battery equivalent circuit model, Ω |
| $R_{con}$ | contact thermal resistance between cell and its plate, $K\,W^{-1}$ |
| $R_t$ | resistance of battery tabs of a cell, Ω |
| $r_p$ | positive electrode resistance, Ω |
| $r_n$ | negative electrode resistance, Ω |
| SOC | state of charge (dimensionless) |
| $t$ | time, S |
| $T$ | temperature, °C |
| $T_{adj,i}$ | adjacent battery cell temperature, °C |
| $T_c$ | lumped battery cell temperature, °C |
| $T_i$ | temperature of cooling fluid at battery pack inlet, °C |
| $T_{max}$ | lumped battery cell peak temperature under simulated US06 cycle, °C |
| $u_\tau$ | friction velocity or shear velocity, $m\,s^{-1}$ |
| $V$ | battery voltage, V |
| $V_c$ | capacitor voltage, V |
| $V_{oc}$ | battery open circuit voltage, V |
| $V_p$ | positive electrode potential, V |
| $V_n$ | negative electrode potential, V |
| $y_p$ | distance between wall surface and the center of prism layer adjacent to the wall surface, m |
| $Z$ | parameter describe battery current density and potential, $V\,m^2\,A^{-1}$ |
| $\nu$ | fluid kinetic viscosity, $m^2\,s^{-1}$ |

Following Gu's approach [8] Shin et al. gave expressions for fitting parameters, $Y$ and $U$, as functions of battery depth of discharge (DOD)

$$U = C_0 + C_1(DOD) + C_2(DOD)^2 + C_3(DOD)^3 \quad (4)$$

$$Y = C_4 + C_5(DOD) + C_6(DOD)^2 \quad (5)$$

where $C_0 \sim C_6$ were the constants that were determined using constant discharge testing data. Considering the charge transfer at the interfaces of electrode and electrolyte and ohmic heating at electrodes, Shin et al. derived the equation of heat generation rate, $q''$, during battery discharge as follows

$$q'' = aJ\left[V_{oc} - (V_p - V_n) - T\frac{dV_{oc}}{dT}\right] + a_p\frac{\nabla V_p^2}{r_p} + a_n\frac{\nabla V_n^2}{r_n} \quad (6)$$

where $a$ was the specific area of the battery while $a_p$ and $a_n$ were the specific area of battery positive and negative electrodes, respectively. It should be noted that the parameter, $Y$, was expressed as the function of only battery depth of discharge (DOD) in Shin et al.'s approach. In other words, the double layer effect or non-faradaic process was not considered in their two-dimension battery model.

In this study, the governing equations of electrode potentials and current density proposed by Shin et al. [5,6] are adopted and extended to the three-dimensional domain. In order to simulate both non-faradaic process and electrochemical reaction or faradaic process and to predict battery behavior under transient charge/discharge cycles, those governing equations are combined with an equation derived from an equivalent circuit model, in which a capacitor is used to describe the double layer effect. Subsequently, these equations are incorporated into a FLUENT CFD battery cell/module level model in the form of User Defined Functions (UDFs) so that battery heat generation rate, convection heat transfer rate, conduction heat transfer rate, and battery temperature can be calculated simultaneously. Finally, a de-coupled three-dimensional battery pack thermal model is developed by incorporating a three-dimensional battery pack flow sub-model without considering the details of battery cells, a one-dimensional battery pack network sub-model, and the battery cell/module level sub-model in which the flow boundary conditions are calculated in the pack flow sub-model. After the battery thermal model is correlated to physical tests, battery cell temperature variation across the pack and non-uniformity of individual battery cell temperatures are studied.

## 2. Battery pack thermal model

Current high-performance computing (HPC) hardware prevents computation of a single transient three-dimensional battery pack thermal model which incorporates the battery heat source equations from thermal behavior prediction under simulated vehicle drive schedules due to extremely large model size and computing memory. Thus, a de-coupled three-dimensional battery pack thermal model has been developed to estimate the temperature contour of individual battery cell units and the lumped temperature variation across entire battery pack. The flow chart of the simulation process is shown in Fig. 1. In order to predict battery pack thermal behavior under simulated vehicle drive schedules (e.g., US06 schedule) using current computing hardware, this approach incorporates a battery cell/module level thermal sub-model, an equivalent circuit sub-model, a one-dimensional network sub-model, and a three-dimensional pack sub-model in which the details of battery cells are not captured. In particular, the convection heat transfer coefficient of individual cooling plate and velocity and pressure profiles at the inlet and outlet of individual cooling channel (Fig. 2) at different battery pack flow rates are calculated in the three-dimensional pack sub-model. The lumped temperature

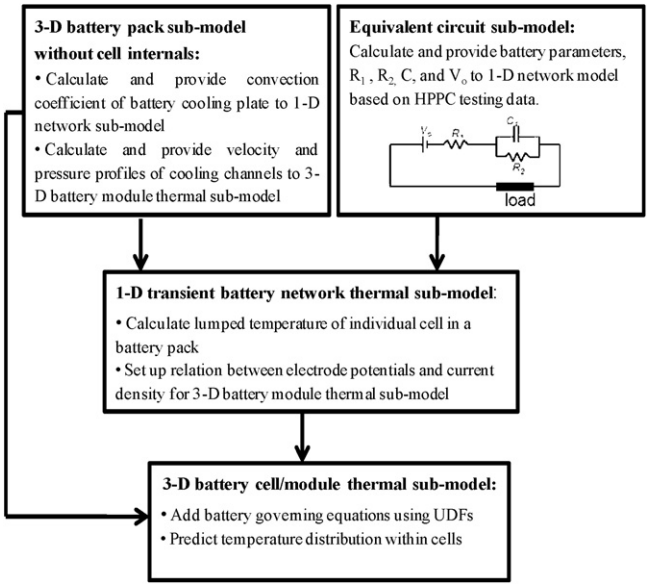


**Fig. 1.** Description of three-dimensional battery pack thermal model.

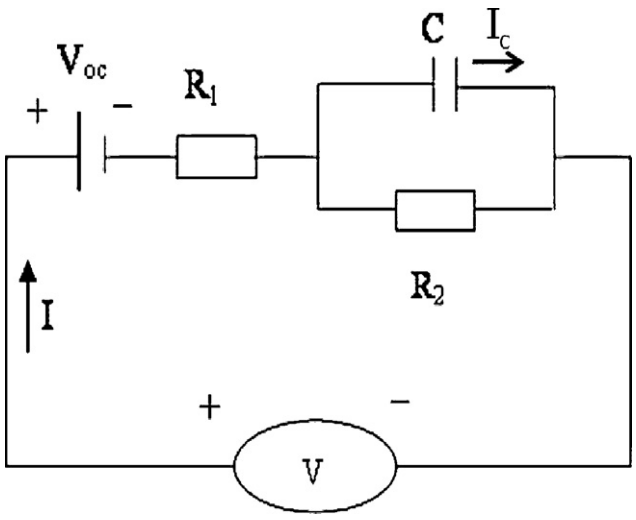


**Fig. 3.** Description of equivalent circuit model.

and the parameter used to describe the relation between electrode potentials and current density of individual battery cells in a pack under various battery charge/discharge cycles are calculated using the one-dimensional battery pack network sub-model combining with an equivalent circuit sub-model. Finally the temperature distribution of battery cells are predicted in the three-dimensional battery cell/module level thermal sub-model, in which the relation between cell electrode potentials and current density estimated in the one-dimensional network sub-model is the input parameter. The flow boundary conditions in the battery cell/module thermal sub-model are established using the velocity and pressure profiles of cooling channels.

### 2.1. Battery pack sub-model

A three-dimensional battery pack sub-model has been initially developed using FLUENT to calculate convection coefficient of cooling plate surface of each individual battery unit [9,10] and velocity and pressure profiles of each cooling channel at different flow rates in a battery pack (Fig. 2). The detail of battery cells are not captured and the battery charge/discharge behavior and thermal behavior thereof are not described in this sub-model to significantly reduce the model size and computing memory requirements. The Reynolds number of the cooling flow channels formed between the battery cooling plates is in the range of 2000–6000 at desired flow rates, so the shear-stress transport (SST) k-omega viscous model [11] is used to calculate the transitional flow properties. The robust and accurate formulation of the k-omega model is applied in the near-wall region, while the free-stream independence of the k-epsilon model is applied in the far field after converting into a k-omega formulation. The function of Low Reynolds Number Correlations is included in the model to accurately simulate the low Reynolds number flows. In order to further improve the accuracy in predicting the convection heat transfer coefficients of battery holder surfaces, three layers of prism elements with equal height are applied in the region near wall surfaces (battery holder surfaces). The height of prism layer is chosen so that the values of wall function $y^+$ ($y^+ = u_\tau y_p/\nu$) are in the range of 0.4–0.8. The velocity and pressure at inlet and outlet of cooling flow channels are saved as profiles and used as the flow boundary conditions in three-dimensional battery cell/module thermal sub-model. The temperature and heat flux of each individual battery cooling surface in a pack are averaged to calculate the lumped convection heat transfer coefficients thereof used in one-dimensional battery pack network sub-model.

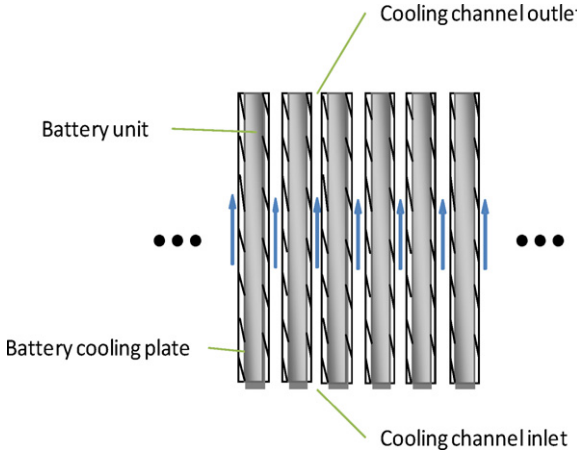


**Fig. 2.** Schematic of battery unit and its cooling channel.

### 2.2. Equivalent circuit and battery pack network sub-models

The relationship between the current, $I$, and voltage, $V$, observed at battery cell terminals can be described using an equivalent circuit model (Fig. 3) [12,13]

$$V - V_{oc} = IR_1 + (I - I_c)R_2 \tag{7}$$

$$I_c = C\frac{dV_c}{dt} \tag{8}$$

Substitution of the solution of Eq. (8) into Eq. (7) and rearrangement give the fundamental equation for battery cell resistance, $R$, during charge or discharge with constant current

$$V - V_{oc} = IR \tag{9}$$

$$R = R_1 + R_2(1 - e^{-t/CR_2}) \tag{10}$$

Battery resistances, $R_1$, and $R_2$, and capacitance, $C$, used to predict the ohmic heat generation rate in one-dimensional battery pack network sub-model are functions of battery SOC (state of charge) and battery cell unit temperature, $T_c$,. The measurements of the battery cell voltage, $V$, open circuit voltage, $V_{oc}$, and current, $I$, are available from HPPC (Hybrid Pulse Power Characterization) tests.

By incorporating the average convection heat transfer coefficient of battery cooling plate surface, $h_{ave}$, estimated from the three-dimensional battery pack sub-model and the battery cell resistances and capacitance calculated using an equivalent circuit model [12,13], the lumped temperature change of each battery cell, $T_c$, in a battery pack under various charge/discharge cycles is calculated using governing equations as follows

$$P = IV \tag{11}$$

$$R_1\frac{dI}{dt} + \frac{I}{C}\left(1 + \frac{R_1}{R_2}\right) = \frac{d(V - V_{oc})}{dt} + \frac{(V - V_{oc})}{CR_2} \tag{12}$$

$$\frac{(T_c - T_{pt})}{R_{con}} - h_a A_p (T_{pt} - T_i) = m_{pt} C_{p,pt}\frac{dT_{pt}}{dt} \tag{13}$$

$$\left[I(V - V_{oc}) + IT\frac{dV_{oc}}{dT}\right] - \frac{(T_c - T_{pt})}{R_{con}} - \sum_{i=1}^{n} k_t A_t \frac{(T_c - T_{adj,i})}{L_t} = m_c C_{p,c}\frac{dT_c}{dt} \tag{14}$$

Here, Eq. (12) is derived from an equivalent circuit model [12,13] shown in Fig. 3. The first term of the left-hand side of Eq. (13) is the conduction heat transfer rate between a battery cell and its cooling plate or holder (Fig. 2). The thermal contact resistance between a battery cell and its cooling plate, $R_{con}$, is estimated based on physical test data. The second term of the left-hand side of Eq. (13) is the convection heat transfer rate between a battery cooling plate and its surrounding cooling fluid.

Since the averaged convection heat transfer coefficient of battery cooling plate surface, $h_a$, is estimated based on the flow temperature at the battery pack inlet in the three-dimensional battery pack sub-model, the flow reference temperature in the second term of Eq. (13) should also be the pack inlet flow temperature, $T_i$. The first term of the left-hand side of Eq. (14) is the battery heat generation rate that involves an irreversible part due to electrochemical polarization and a reversible part due to entropy change [3,6,14]. The reversible part of heat generation rate is proportional to the gradient of the battery cell open circuit voltage, $dV_{oc}/dT$. The conduction heat transfer rate between a battery cell unit and its connecting cell units (Fig. 2) is also considered in the model and presented as the third term of the left-hand side of Eq. (14). Eqs. (11)–(14) are solved using 4th order Runge–Kutta method.

The parameter used to describe the relation between current density and electrode potentials in the three-dimensional battery cell/module thermal sub-model is also estimated in terms of battery cell current and voltage, i.e.,

$$Z = NA_e\left(\frac{\left|V - V_{oc}\right|}{I} - R_t\right) \tag{15}$$

The battery double layer effect is considered using a capacitor in the model as shown in Fig. 3 to describe the effect of charge/discharge time and change of current on battery cell voltage change.

### 2.3. Battery cell/module thermal sub-model

The governing equations of electrode potentials (1) and (2) adopted from Shin et al.'s approach [5,6] are used in the three-dimensional battery cell/module thermal sub-model. Based on the descriptions by Shin et al. [5,6] and Gu [8], the relation between current density and potential difference is rearranged as follows

$$J = \frac{V_p - V_n - V_{oc}}{Z} \tag{16}$$

Here, the parameter, $Z$, is calculated using the one-dimensional battery pack network sub-model in which the battery double layer effect is considered. Following the approaches used by Shin et al. [5,6] and Srinivasan and Wang [15], the heat generation rate of the battery active material region, $q''$, is given as

$$q'' = \frac{\nabla V_p^2}{L_e r_p} + \frac{\nabla V_n^2}{L_e r_n} + \frac{C_q}{L_e}J\left[V_p - V_n - V_{oc} - T\frac{dv_{oc}}{dT}\right] \tag{17}$$

where $L_e$ is the distance between the centerlines of positive and negative electrode current collectors for a battery cell with double-sided electrodes. For example, $L_e$ includes the thicknesses of one-half of positive electrode current collector, one side of cathode, one separator, one side of anode, and one-half of negative electrode current collector. The first and second terms of the right-hand side of Eq. (17) are the heat rates generated due to the gradient of positive potential and the gradient of negative potential, respectively [5,6]. The parameter, $C_q$, is introduced at the third term of the right-hand side of Eq. (17) to offset the portion due to the gradients of electrode potentials from the total heat generation rate. So this term represents the heat generation rate due to the charge transfer at the electrode/electrolyte interface. The heat rate generated at the battery tabs, $q_t''$, is given as

$$q_t'' = \frac{I^2 R_t}{A_t L_t} \tag{18}$$

Eqs. (1), (2), (16), (17), and (18) are incorporated into FLUENT thermal sub-model using user defined functions (UDFs) and solved simultaneously with the energy equation in the FLUENT sub-model. In particular, governing Eqs. (1) and (2) are defined as scalar transport equations while Eq. (16) is used as a global function and Eqs. (17) and (18) are used as heat source terms in UDFs.

Similar to the battery pack sub-model the shear-stress transport (SST) k-omega viscous model [11] with the function of Low Reynolds Number Correlations has been used to calculate the transitional flow properties. The flow boundary conditions in the sub-model are the velocity and pressure profiles at inlet of cooling channel and the pressure profile at outlet of cooling channel that are calculated in the battery pack sub-model.

### 2.4. Battery thermal model correlation

The convection heat transfer rate of battery cooling plate surface and battery heat generation rate are the two major parameters that affect the temperature of battery cells. The estimation of convection heat transfer rate between battery cooling plate surface and cooling fluid was verified by measuring battery cooling plate temperature changes following a designed testing procedure, i.e., the baseline battery pack was heated to above 35 °C, then the cooling fan of the battery pack was turned on to cool down the battery cells at constant inlet flow rate of 60 CFM or 80 CFM. The charge/discharge power of the battery pack was cut off during the cooling process so that the effect of the battery heat source could be isolated. Thus, the convection heat transfer rate between the battery cooling plate surface and cooling fluid was the only major source to affect the temperature of battery cell and its cooling plate. By selecting appropriate transitional flow treatments including meshing elements as discussed in the three-dimensional battery pack sub-model, the estimated convection heat transfer rates between battery cooling plate surface and the cooling air were in good agreement with the experimental data. As an example, the comparisons of analytical and experimental temperature changes of battery cooling plates with the highest averaged convection heat transfer rate and lowest averaged convection heat transfer rate in the baseline battery pack are shown in Fig. 4(a) and (b), respectively. It is found that the maximum deviation of the convection heat transfer coefficient of battery cooling plate between simulation and test is less than 5%.

The material properties and states of charge of battery cells in a pack are assumed the same. Thus, the distribution of heat

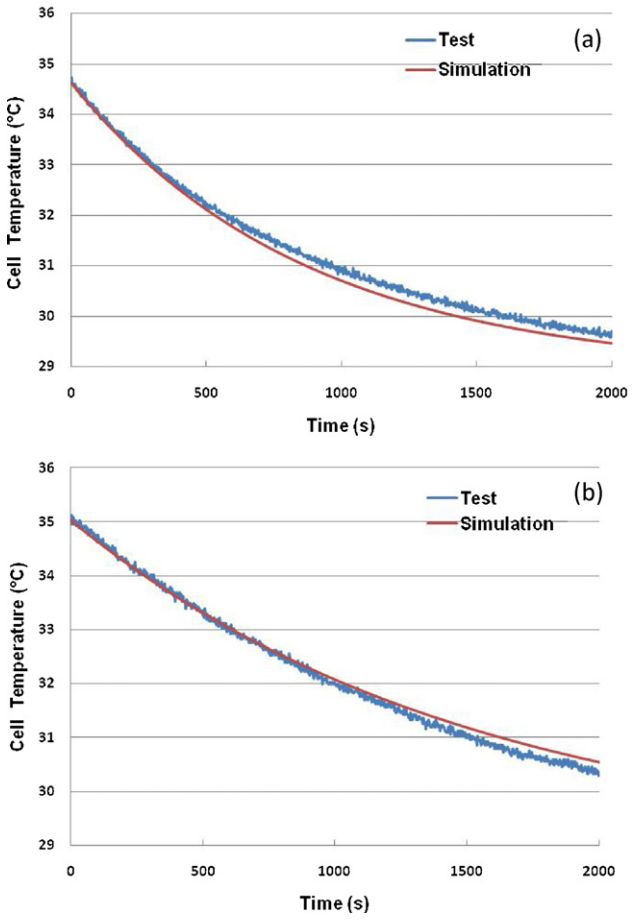


**Fig. 4.** Battery cooling correlation at inlet flow rate of 60 CFM, (a) cooling plate with the highest $h_a$ in the pack, (b) cooling plate with the lowest $h_a$.

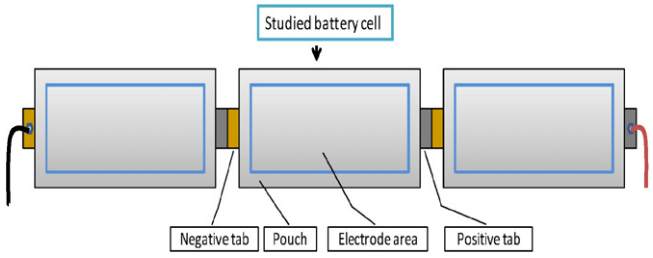


**Fig. 5.** Connection of battery cells.

generation rate of each battery cell in a pack was verified by measuring the temperature distribution of a single battery cell under square wave charge/discharge cycles. In order to create the same heat conduction boundary condition as that in the battery pack, positive and negative tabs of the studied battery cell were connected to the corresponding tabs of other two battery cells using ultrasound welding (Fig. 5). The battery cell surfaces were exposed in an environment in which the convection fluid motion was due to buoyancy force. The free or natural convection coefficients at different positions of battery cell surface were approximately 4.5 ($W\,m^{-2}\,K^{-1}$) as battery cell temperature was increased by about 10 °C. Initially the battery cell was charged or discharged to achieve the state of charge (SOC) to be around 50%. After at least 1 h rest to allow the cell to return to an equilibrium condition, the cell voltage was measured to determine exact initial SOC (at $t = 0$ s) based on the SOC – open circuit voltage curve. The formal test was then performed with 6C rate of square wave charge/discharge cycles, i.e., both discharge current and charge current were approximately 31 A. The time period of one square wave charge/discharge cycle was 60 s. The cut-off voltages were set to 2.5 V during discharge and 4.3 V during charge, respectively.

An infrared thermal camera with 0.1 °C temperature indication resolution was used to capture the temperature image of the studied battery cell. The comparisons of analytical and experimental

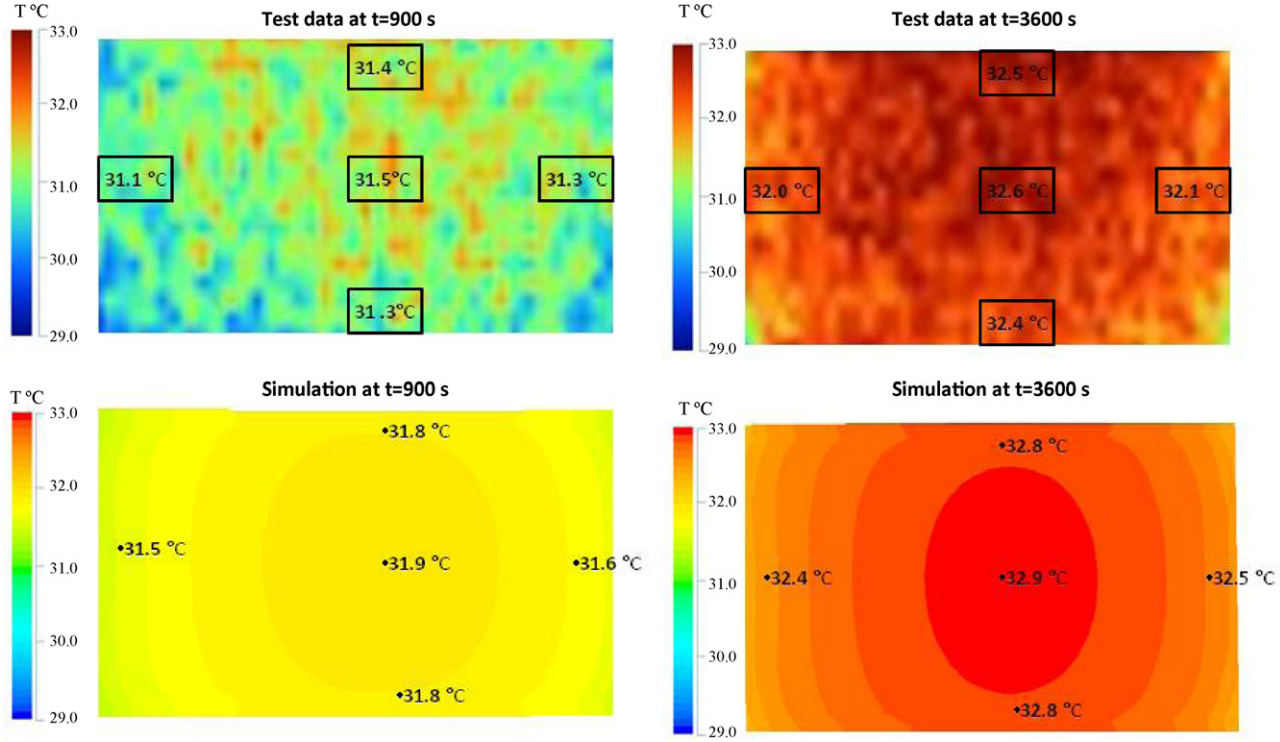


**Fig. 6.** Analytical and experimental temperature contours of studied battery surface.

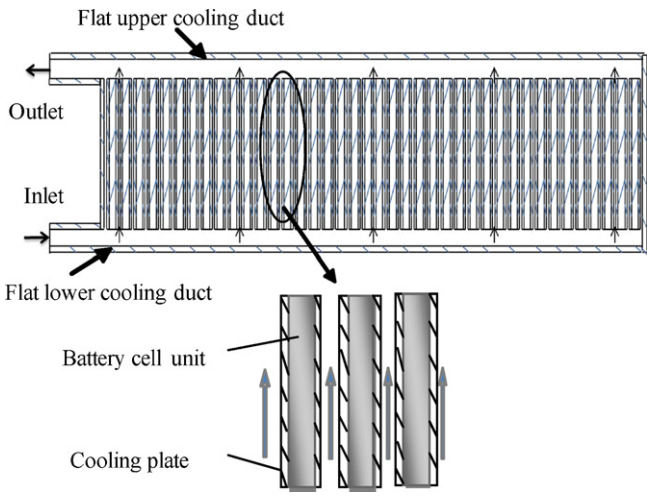


**Fig. 7.** Schematic of a baseline "U-type" flow battery pack.

temperature contours of the battery surface at 900 s and 3600 s under square wave charge/discharge circles are shown in Fig. 6. As can be seen, the predicted temperature distributions of battery cell surface are in agreements with the physical tests. The central region has highest temperature and the maximum temperature variation of the battery cell surface is approximately 0.6 °C when battery cell temperature is increased by approximately 10 °C. It is also found that the temperature of the region close to the positive tab is about 0.1 °C higher than that at negative tab side.

## 3. Results and discussions

Numerical simulations are performed in a battery pack to study the battery temperature variation across the pack and non-uniform temperature within individual battery cells. The baseline battery pack includes 40 battery units and cooling plates and lower and upper cooling ducts. The heights of upper and lower cooling ducts are constant and approximately the same. As indicated by arrows shown in Fig. 7, the cooling air from the pack inlet enters the lower cooling duct and passes through the cooling channels between two adjacent battery cooling plates to facilitate heat transfer from the outer planar surfaces of the battery units to the fluid. The hot air exits from the upper cooling duct through the pack outlet. The pack inlet and outlet are located at the same side to form "U-type" flow in the pack. In this pack battery cell unit 1 is adjacent to the pack inlet/outlet, and unit 40 is located at the other side of the battery pack. In order to address the worst battery pack thermal behavior, the battery pack power input in the de-couple battery pack thermal model is based on simulated US06 driving cycles, an aggressive driving pattern with high engine/battery loads.

### 3.1. Temperature variation across pack

The transient lumped temperatures of battery cell units in the baseline battery pack under US06 driving cycle are calculated using the battery pack sub-model and one-dimensional transient battery pack network sub-model. As an example, the lumped temperature changes of hottest and coldest battery units in the pack at the inlet flow rate of 60 CFM are shown in Fig. 8(a) and (b), respectively. As can be seen the analytical transient temperatures of battery cells are in good agreement with test data. After 5000 s the convection heat transfer rate and heat generation rate tend to be approximately balanced during each US06 cycle and the temperature of each battery unit fluctuates around a certain value. It should be noted that the

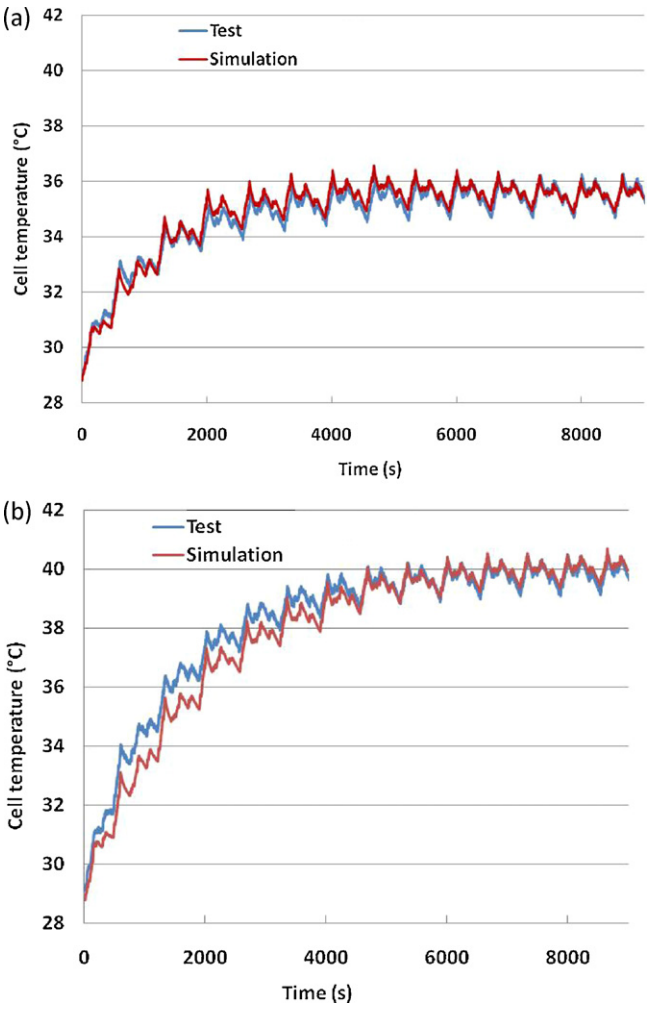


**Fig. 8.** Transient battery unit temperature at inlet flow rate of 60 CFM, (a) coldest cell and (b) hottest cell.

test data is the average temperature measured at four positions of each cooling plate. Due to small thickness and high conductivity of the cooling plate and relatively high contact pressure between the cooling plate and the battery cell the temperature of cooling plate is approximately the same as battery unit surface temperature at same position. Fig. 9(a) and (b) show the maximum or peak temperatures of individual battery units at inlet flow rates of 60 CFM and 80 CFM, respectively. It is found that the temperatures of battery units at the inlet/outlet side of the battery pack are approximately 4 °C lower than the temperature of battery units at the other side of the battery pack under US06 driving cycles. This is because the flow separations occurred at the upper duct as the cooling air flowed out from the cooling channels [16]. The flow separations in the upper duct and the friction effect in the lower and upper ducts caused the pressure drops in the cooling channels at right side of the battery pack shown in Fig. 7 to be lower than those at the inlet/outlet side of the pack. As a result, flow rate and surface convection coefficient of the cooling channels at right side of the battery pack are smaller than flow rates and surface convection coefficients of the cooling channels at the inlet/outlet side of the pack, which in turn causes the temperature of battery units at the right side of the pack to be higher [9].

Thus, the variation of battery temperatures across the battery pack can be reduced by improving uniformity of the pressure drops in the cooling channels. Simulation results indicate a tapered upper cooling duct shown in Fig. 10 can reduce the flow pressure in the

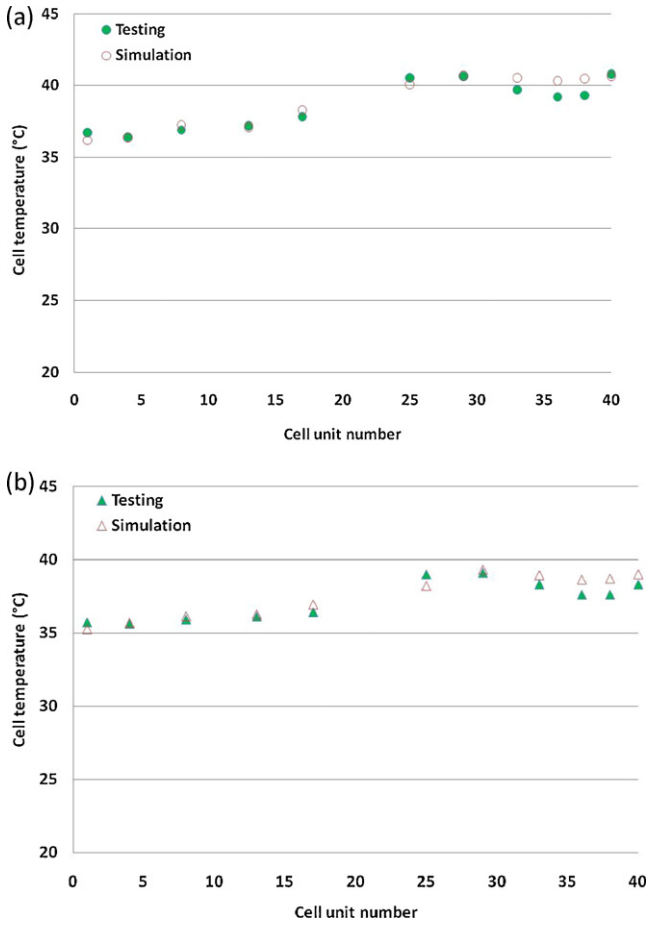


**Fig. 9.** Maximum temperature of individual battery cells in the baseline pack at inlet flow rates of (a) 60 CFM and (b) 80 CFM.

area of the upper duct at the right side. As a result, the pressure drops in the cooling channels at right side of the battery pack tend to be the same as those at inlet/outlet side. As an example, by modifying an upper cooling duct with an appropriate taper angle the estimated maximum temperature variation of battery units across the modified pack under US06 driving cycles at inlet flow rate of 60 CFM is reduced from 4.0 °C to 1.3 °C, which is in good agreement with physical test data (Fig. 11) that is 1 °C.

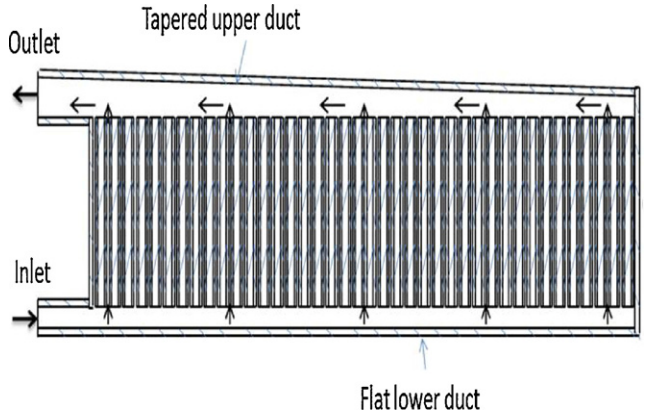


**Fig. 10.** Schematic of a tapered "U-type" flow battery pack.

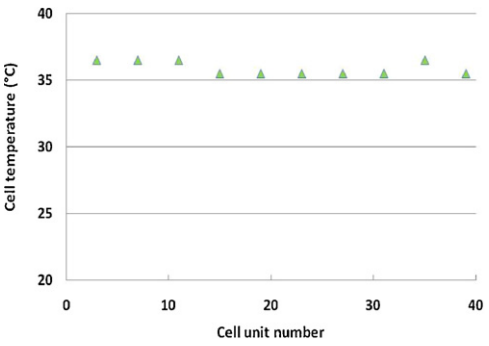


**Fig. 11.** Measured peak temperature of battery cells in modified "U-type" flow battery pack at inlet flow rate of 80 CFM under US06 cycles.

### 3.2. Temperature variation within a battery cell

The temperature variation within each battery cell and the root cause are studied in the modified "U-type" battery pack by incorporating the transient three-dimensional battery cell/module thermal model with the battery pack sub-model and one-dimensional transient battery pack network sub-model. As an example, the contour of temperature of the hottest battery cell in the pack at the inlet flow rate of 60 CFM under simulated US06 diving cycles is shown in Fig. 12. It can be seen that the hot spots occur at the top edge of battery cell while the bottom edge of battery cell has lowest temperature. The maximum temperature variation on the battery cell surface is approximately 2 °C. This is because the flow velocity is approximately the same while the temperature of the fluid gradually increases along vertical direction as the cooling air flows vertically in the cooling channel with constant gap (Fig. 7). The temperature of the fluid at the exit of the cooling channel tends to be the same as the temperature of the top surface of the battery cell due to the small cooling channel gap and relatively low flow rate. As a result, the heat transfer rate of the bottom surface of battery cell is much larger than that of the top surface, which in turn causes the battery cell surface temperature to be increased gradually along the vertical direction. Although the heat generation rate is not uniform within a battery cell, it has been shown that the temperatures of top edge and bottom edge are approximately the same and the maximum temperature variation is only about 0.6 °C by applying approximately uniform convection heat transfer rates on battery cell surface (Fig. 6). Thus, the large non-uniformity of the convection heat transfer rate of cooling plate surface plays the major role on the battery cell temperature variation particularly at high pack inlet flow rate.

Solutions have been investigated to reduce the temperature variation within individual battery cells in the pack without significantly changing the pack design and increasing the lumped battery cell temperature. As an example, it is found that the temperature

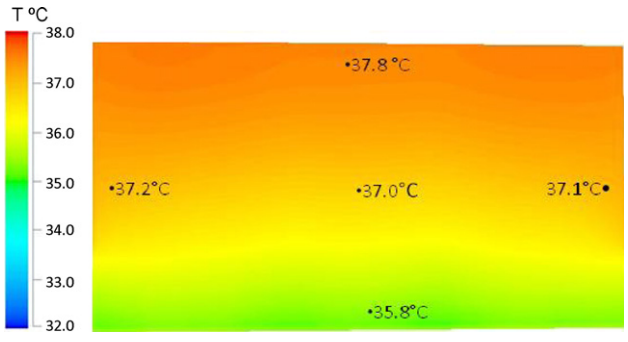


**Fig. 12.** Temperature contour of battery cell surface.

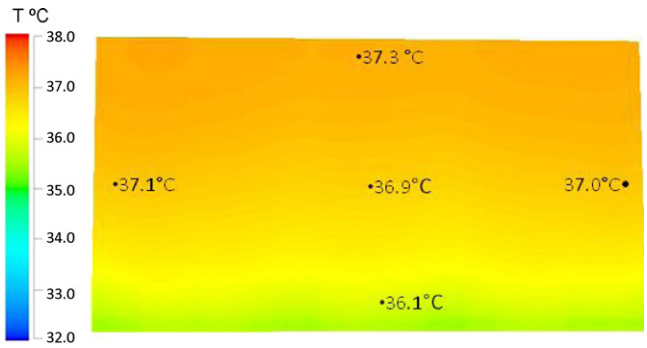


**Fig. 13.** Temperature contour of battery cell with higher heat thermal conductivity.

variation within the same cell surface in the pack can be reduced from 2 °C to 1.2 °C by increasing the thermal conductivity of battery cell [17] in the in-plane direction by 100% as shown in Fig. 13.

## 4. Conclusions

A decoupled three-dimensional battery pack thermal model has been developed to estimate the temperature variation of battery cells across a pack and temperature contours of individual battery cells in a pack. This decoupled approach incorporates a steady three-dimensional battery pack sub-model, an equivalent circuit sub-model, a one-dimensional battery pack network sub-model, and a three-dimensional battery cell/module thermal sub-model. In the three-dimensional battery cell/module thermal sub-model the governing equations of electrode potentials and current density proposed by Shin et al. are adopted and extended to three-dimensional domain. By combining those equations with the equations used in an equivalent circuit sub-model and a battery pack network sub-model, both non-faradaic process and electrochemical reaction or faradaic process of individual battery cells can be simulated to predict battery behavior under transient charge/discharge cycles. Good correlation with physical tests has been confirmed.

Simulations indicate that the geometry of cooling ducts can significantly affect the battery temperature uniformity across a pack. In particular, the maximum temperature variation of battery units in a baseline battery pack can be improved by approximately 70% by using a tapered upper cooling duct, which is confirmed by the physical test data. Simulations also indicate that the temperature variation within each battery cell can be approximately 2 °C though the lumped temperature variation of battery cells across the pack is only around 1 °C. The large temperature variation within a cell is mainly caused by the large non-uniformity of the convection heat transfer rate on the cooling surface especially at high pack inlet flow rates.

## Acknowledgments

The authors would like to thank Daniel Brouns, Christopher Ciaramitario, Eric Losiewicz, Ramona Ying, Christopher Mousseau, and Andrew Herman for their valuable help and providing the physical test data.

## References

[1] J. Newman, W. Tiedemann, AIChE J. 21 (1975) 25–41.
[2] C.Y. Wang, W.B. Gu, B.Y. Liaw, J. Electrochem. Soc. 145 (1998) 3407–3417.
[3] W.B. Gu, C.Y. Wang, J. Electrochem. Soc. 147 (2000), 9010-2922.
[4] L. Cai, R. White, J. Electrochem. Soc. 156 (2009) 154–161.
[5] K.H. Kwon, C.B. Shin, T.H. Kang, C.S. Kim, J. Power Sources 163 (2006) 151–157.
[6] U. Kim, C. Shin, C. Kim, J. Power Sources 180 (2008) 909–916.
[7] J. Newman, W. Tiedemann, J. Electrochem. Soc. 140 (1993) 1961–1968.
[8] H. Gu, J. Electrochem. Soc. 130 (1983) 1459–1464.
[9] H. Sun, B. Tossan, and D. Brouns, SAE 2011-01-1368 (2011).
[10] H. Sun, Res. Disclosure (2009) 542084.
[11] ANSYS FLUNET 12.0 Theory Guide, ANSYS Inc.
[12] M. Verbrugge, E. Tate, J. Power Sources 126 (2004) 236–249.
[13] M. Verbrugge, R. Ying, J. Electrochem. Soc. 154 (2007) 949–956.
[14] N. Sato, J. Power Sources 99 (2001) 70–77.
[15] V. Srinivasan, C.Y. Wang, J. Electrochem. Soc. 150 (2003) 98–106.
[16] D.S. Miller, Internal Flow Systems, 2nd edition, Gulf Publishing Company, Houston, USA, 1990.
[17] H. Maleki, J.R. Selman, R.B. Dinwiddie, H. Wang, J. Power Sources 94 (2001) 26–35.